**Astronomy**
**&**
**Astrophysics**

# A synthetic stellar polarization atlas from 400 to 1000 nm[*]

H. Socas-Navarro[1], A. Asensio Ramos[2], and R. Manso Sainz[2]

[1] High Altitude Observatory, NCAR[**], 3080 Center Green Dr, Boulder CO 80301, USA
  e-mail: `navarro@ucar.edu`
[2] Instituto de Astrofísica de Canarias, Avda Vía Láctea S/N, La Laguna 38200, Tenerife, Spain

**ABSTRACT**

*Context.* With the development of new polarimeters for large telescopes, the spectro-polarimetric study of astrophysical bodies is becoming feasible and, indeed, more frequent. In particular, this is permitting the observational study of stellar magnetic fields.
*Aims.* With the aim to optimize and interpret this kind of observations, we have produced a spectral atlas of circular polarization in a grid of stellar atmospheric models with effective temperatures between 3500 and 10 000 K, surface gravities $\log(g) = 3.5-5$, metallicities between $10^{-2}$ and 1, and magnetic field strengths of 100, 1000 and 5000 G.
*Methods.* We have computed the emergent Stokes $I$ and $V$ flux spectra in LTE of more than $10^5$ spectral lines.
*Results.* The atlas and several numerical tools are available in electronic format and may be downloaded from `http://download.hao.ucar.edu/pub/PSA/`. In this paper we review and discuss some of its most relevant features, such as which spectral regions and individual lines harbor the strongest signals, what are interesting lines to observe, how to disentangle field strength from filling factor, etc.

**Key words.** atlases – stars: atmospheres – stars: magnetic fields – line: formation – polarization – radiative transfer

## 1. Introduction

The development of large-aperture telescopes and high-sensitivity polarimetric instrumentation is providing the Astrophysical community with new tools to explore the universe. Polarimetric observations are opening new and exciting possibilities for the diagnostics of light-matter interaction processes in many different scenarios (see, e.g., the various reviews in Trujillo Bueno et al. 2002).

There are two major reasons why spectral lines produced in stellar atmospheres may become polarized. First, we may have scattering processes in which the photons emitted by the source are deflected towards Earth. Depending on the details of the interaction, one receives light that is (at least in part) linearly polarized in a direction that is closely related to the scattering geometry (and some times other factors, such as the magnetic field). This is obviously of great interest for the detection and characterization of exoplanets (e.g., Keller 2006), protoplanetary and accretion disks (e.g., Donati et al. 2005; Hales et al. 2006; Perrin et al. 2006), binary systems (e.g., Landi degl'Innocenti et al. 1988) etc.

Another source of polarized light is the Zeeman effect that splits the atomic energy sublevels when magnetic fields are present in the spectral line formation region. The strength of the magnetic field required to produce a certain amount of polarization depends on details of the radiative transfer (Zeeman

sensitivity of the spectral lines, opacity profile, source function gradient, etc.). Angular integration of a spherically-symmetric emitting source results in circular polarization spectral profiles (linear polarization would cancel out). Analysis of these spectral profiles provides unvaluable clues to study, e.g. magnetic activity in stars (e.g., Wade et al. 2005; Shakhovskoj et al. 2006).

For several decades now, the grid of radiative equilibrium model atmospheres and spectra computed by Kurucz (for an updated reference see Castelli & Kurucz 2003) have been very useful in the preparation and interpretation of stellar observations. We felt that a polarization atlas of the signal emergent from those models, for several magnetic field strengths and metallicities, would also be useful for future observations of stellar magnetic fields. The entire grid of polarized spectra computed in this work is publicly available for download from the following URL: `http://download.hao.ucar.edu/pub/PSA/`.

## 2. The atlas

The synthetic spectra have been obtained using a compilation of spectral line data from Kurucz & Bell (1995) between 400 and 1600 nm for the model with $T_{\rm eff} = 5750$ K and $\log(g) = 4.5$ (hereafter, the solar-like model), and between 400 and 1000 nm for the rest (if there is enough interest, we may consider extending the wavelength range). This is a useful range to consider, as it is accessible to modern spectro-polarimetric instruments such as MUSICOS (Donati et al. 1999) or ESPaDOnS (Manset & Donati 2003).

Due to insufficient data on partition functions we restricted ourselves to lines of up to the third ionization stage. Lines of higher ionization stage have been excluded. The effective Landé

---

**Table 1.** Number of lines included and excluded in the syntheses.

| Wavelength range (nm) | Lines considered | Lines excluded | Lines set to $\bar{g}_{\text{eff}} = 0$ |
|---|---|---|---|
| 400.00–499.99 | 40 343 | 835 | 8263 |
| 500.00–599.99 | 27 849 | 421 | 6396 |
| 600.00–699.99 | 20 371 | 192 | 4549 |
| 700.00–799.99 | 16 141 | 215 | 2915 |
| 800.00–899.99 | 12 793 | 104 | 2286 |
| 900.00–999.99 | 11 297 | 92 | 2779 |
| 1000.00–1099.99 | 8601 | 43 | 2138 |
| 1100.00–1199.99 | 6821 | 67 | 1499 |
| 1200.00–1299.99 | 6016 | 54 | 1280 |
| 1300.00–1399.99 | 5357 | 26 | 1015 |
| 1400.00–1499.99 | 5153 | 17 | 948 |
| 1500.00–1599.99 | 4759 | 24 | 974 |

factor ($\bar{g}_{\text{eff}}$) for lines that are not well described by the *LS* coupling or for which there is no level configuration information has been set to zero, so no polarization signal will appear in these lines[1]. Following Casini & Landi Degl'Innocenti (1994), the H$\alpha$ line is assumed to have an effective Landé factor of 1. A comprehensive list of the lines excluded or computed with zero Landé factor (35 042 for the solar-like model and 27 188 for the others) is available for download in electronic format. The total number of lines considered is 165 501 in the extended range for the solar-like model and 128 794 for all others. Table 1 lists the distribution of spectral lines included and excluded in each wavelength range.

The full polarized radiative transfer vector equation for a given wavelength is usually written as:

$$\frac{\text{d}\boldsymbol{I}(s)}{\text{d}s} = -\mathbf{K}(s)[\boldsymbol{I}(s) - \boldsymbol{S}(s)], \qquad (1)$$

where $s$ is the distance along the ray path, $\boldsymbol{I}$ is the Stokes vector, $\boldsymbol{S}$ is the source function vector (which in LTE is usually the Planck function times the transpose of the unitary $[1, 0, 0, 0]$ vector), and finally $\mathbf{K}$ is the absorption matrix:

$$\mathbf{K} = \begin{pmatrix} \eta_I & \eta_Q & \eta_U & \eta_V \\ \eta_Q & \eta_I & \rho_V & -\eta_U \\ \eta_U & -\rho_V & \eta_I & \rho_Q \\ \eta_V & \rho_U & -\rho_Q & \eta_I \end{pmatrix}. \qquad (2)$$

For details on the meaning of the symbols employed in the equations above, the reader is referred to Landi Degl'Innocenti & Landolfi (2004). Note that, although we are only interested on the emergent intensity $I$ and circular polarization $V$, we must compute all the four Stokes parameters consistently due to the off-diagonal terms in $\mathbf{K}$.

The syntheses were carried out using a modified version of the code LILIA (Socas-Navarro 2001). This code was designed for the synthesis and inversion of polarized atomic spectral lines formed in LTE (molecular bands cannot be treated with this code). Solar metal abundances are those from Anders & Grevesse (1989). For all other metallicities, abundances are scaled by a constant factor. Background opacities are obtained with the opacity package used by Shchukina & Trujillo Bueno (2001). The atmosphere is assumed to be one-dimensional and plane-parallel. The formal solution of the polarized transfer

---

[1] Although we shall often refer to effective Landé factors, our computation actually takes into account the full Zeeman pattern (anomalous splitting) and does not resort on the triplet approximation.

equation is based on the Hermitian method of Bellot Rubio et al. (1998). However, a much simpler method may sometimes be used (see the Weakly Polarizing Media approximation below).

The plane-parallel approximation is justified by our choice of not considering the largest stellar models (log($g$) between 3.5 and 5). The LTE approximation implicit in the expressions of the source function and the absorption matrix is justified by the range of effective temperatures, $T_{\text{eff}}$ between 3500 and 10 000 K.

For consistency, we started with the mass scale from the original models and transformed it into an optical depth scale, using our opacities in the calculation. The optical depths obtained are the reference height scale for the radiative transfer. In order to avoid very hot (where LTE may not be a good approximation for many photospheric lines) or very large stars (where the spherical geometry may be needed), we decided to restrict ourselves to a range of effective temperatures (hereafter $T_{\text{eff}}$) between 3500 and 10 000 K and surface gravities (hereafter log($g$)) between $10^{3.5}$ and $10^5$. The mixing-length treatment of these models has been described by Casteli et al. (1997b, see also Casteli et al. 1997a).

We selected five different representative metallicities, with abundance ratios (relative to solar) of 1, $10^{-0.5}$, $10^{-1}$, $10^{-1.5}$, and $10^{-2}$. For each abundance, $T_{\text{eff}}$ and log($g$), we computed three different magnetic field strengths of 100 G, 1000 G and 5000 G.

It is clear that the amount of all possible realizations of magnetic field configurations on the surface of a star cannot be exhausted by any reasonable grid of models; that is certainly not the aim of this work. To find out the particular configuration that best fits some observation, one would need to resort on least-squares inversion methods (such as that of Allende Prieto et al. 2000). Our atlas has been calculated to give a qualitative account of actual observations, as well as to explore possible observational strategies, find the most promising spectral lines for magnetic field diagnostics, etc. Therefore, we have assumed the simplest possible configuration, given by a monopolar magnetic field pointing radially away from the center and of constant strength.

The spectra are calibrated in flux using a 3-point Gaussian quadrature. We looked at several randomly-chosen models and verified that increasing the quadrature grid to 4 or 5 points did not make any significant difference.

The models used here have a depth-independent microturbulent velocity of 2 km s$^{-1}$ and a macroturbulence of 1 km s$^{-1}$. These are roughly representative solar values . In addition to turbulence, other line-broadening mechanisms are taken into account after Gray (1976):

- radiative broadening. We set $\Gamma_r = 0.22233/\lambda^2$ (with $\lambda$ in cm). This formula is only a rough approximation but radiative broadening is usually very small anyway;
- Van der Waals broadening. Note that the Gray (1976) expressions are only accurate for neutral or singly ionized atoms. For other ions we neglect this broadening;
- Stark broadening. We use the approximation $\Gamma_S \simeq 10.06666 + \log_{10}(P_e) - 5/6 \log_{10}(T)$, where $P_e$ and $T$ are the electron pressure and the local temperature (in cgs units).

Even assuming LTE, the synthesis of the Stokes profiles of over $10^5$ spectral lines in a large grid of model atmospheres is a very demanding computing task. To bring the computing time within reasonable practical limits we implemented a number of optimizations that do not harm significantly accuracty of the polarized spectra:

- *Background opacities.* These are not recomputed at each wavelength. Instead, they are evaluated every 0.1 nm. This
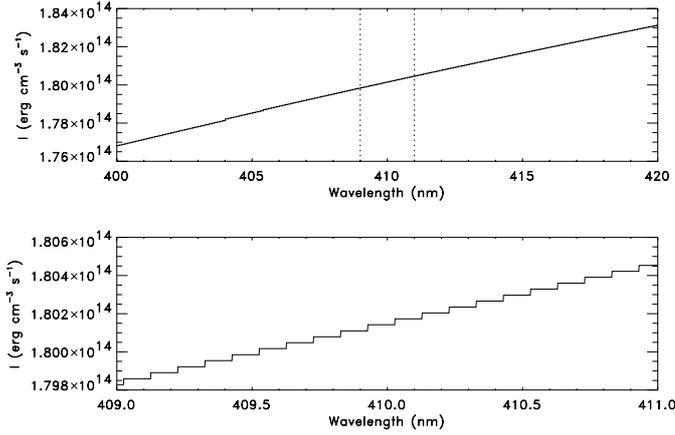
**Fig. 1.** Blue continuum spectrum for the solar-like model. The lower panel shows a close-up of the region marked by vertical dotted lines in the upper panel, rescaled to show the discretization of the continuum. Notice, however, in the ordinates scale that this effect is very small.



**Fig. 2.** Spectral profile of the Ca II line in the solar-like model, showing some small glitches (marked by the arrows) in the line-to-continuum transition of Stokes *I* (*upper panel*). Stokes *V* (*lower panel*) is much less sensitive to this effect.

is noticeable, e.g. when one inspects closely the continuum intensity over a very short wavelength range. Figure 1 shows the continuum for the solar-like model. A very close zoom-in reveals the discretization in the continuum caused by this approximation. Notice, however, the ordinates scale which shows that the continuum is virtually flat and thus the error introduced (the "step" of the staircase) is very small, at the $10^{-4}$ level.

– *Weak lines.* Depending on the particular physical conditions on a given atmosphere, many spectral lines turn out to be negligibly weak. Removing these lines from the computation saves a large amount of processing power. We implemented a criterion, according to which a line is ignored if its line-core opacity is at most 10% larger than the continuum opacity at all depth-points in the atmosphere. The line-core opacity is calculated as:

$$\eta_0 = 4.9947 \times 10^{-21} \frac{10^{\log(g_l f)}(n_l - n_u)}{\rho \Delta \lambda_D^2}, \tag{3}$$

where $g_l$ is the statistical weight of the lower level, $f$ is the oscillator strength, $n_l$ and $n_u$ are the atomic lower and upper level number densities, $\rho$ is the gas density and $\Delta \lambda_D$ is the Doppler width (see Eq. (4) below). If all these parameters are given in cgs units, the resulting $\eta_0$ is in units of cm$^2$ g$^{-1}$.

– *Line profiles.* Computing Voigt functions (Humlicek 1982) for a large number of lines, wavelength points and many Zeeman components is the dominant fraction of the spectral synthesis time, even when using an optimized vector routine. Extending the Voigt profiles too far into the wings results in a lot of unnecessary processing. On the other hand, falling short produces inaccuracies near the continuum. A good estimate of the width of the line is therefore very important in optimizing the efficiency of the code. We have implemented an adaptive scheme that starts with a standard width of 0.01 nm and extends the interval until the opacity at the boundaries is smaller than 1% of the continuum opacity. Figure 2 shows the Ca II line at 854.2 nm in the solar-like model. This is perhaps the line that shows the most conspicuous glitch (marked by arrows in the figure) in the transition from line to continuum. The glitch is noticeable only marginally in Stokes *I* and is negligible in Stokes *V*.
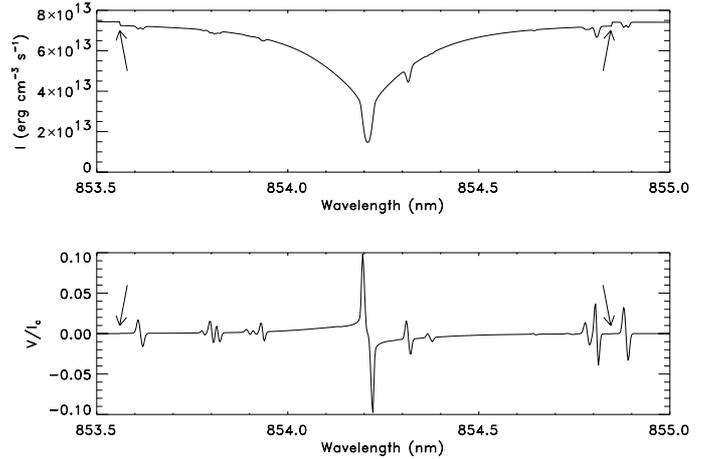
– *Wavelength sampling.* Since the Doppler width of the lines increases with wavelength (and the Zeeman splitting increases with the square of the wavelength), one needs more resolution in the blue than in the red side of the spectrum. We divided the spectra in 100 nm intervals and used a sampling typical of solar observations in the visible ($\simeq$20 mÅ at 650 nm). This sampling is then scaled linearly with wavelength. It may be seen that even for cool atmospheres and relatively heavy ions our sampling is still smaller than the Doppler width of the lines, given by:

$$\Delta \lambda_D = \lambda \left( \sqrt{\frac{2kT}{m_A}} + \frac{v_{\text{mic}}}{c} \right), \tag{4}$$

where $k$ is the Boltzmann constant, $T$ is the temperature in the atmosphere, $m_A$ is the atomic mass, $v_{\text{mic}}$ is the microturbulence and $c$ is the speed of light.

– *Weakly Polarizing Media.* In many cases, the radiation field is weakly linearly polarized, while $\eta_{Q,U}/\eta_I \ll 1$, and magneto-optical terms are negligible ($\rho_{Q,U,V}/\eta_I \ll 1$). In those cases, the coupled system of Eq. (1) simply reduces to two decoupled differential equations for $I \pm V$ that are easily integrated. If circular polarization is also weak, we can neglect the $-\eta_V V$ from the equation for the intensity (this is the Weakly Polarizing Media approximation of Sánchez Almeida & Trujillo Bueno 1999) and we get an independent equation for the intensity $I$, and an easily integrable equation for $V$. If the criterion above is satisfied for all depth-points in the atmosphere, the code automatically switches to this method for the formal solution.

## 3. Discussion

Because the Zeeman splitting increases with wavelength, one might expect infrared regions to be more promising targets for magnetic field observations. However, this is not necessarily the case. Figure 3 shows the total amount of polarization (in absolute value) measured in each 100 nm interval of the solar-like model spectrum, i.e., $\int_{\lambda_0}^{\lambda_1} |V(\lambda)|/I_c(\lambda) d\lambda$. By far, the blue side of the spectrum carries a much higher density of polarization signal than the red or infrared. In fact, for the strongest fields, the
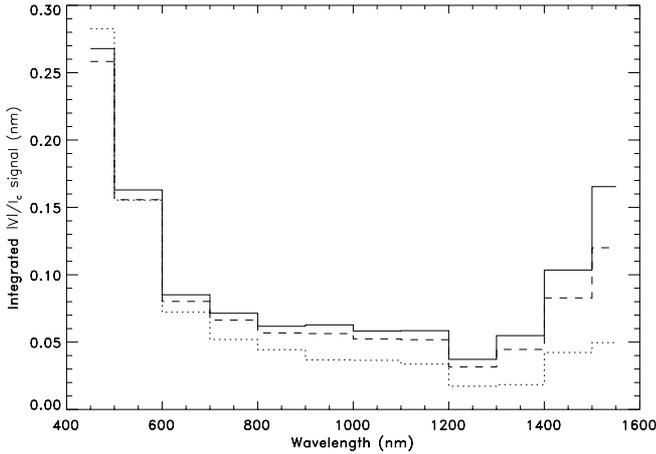
**Fig. 3.** Integrated absolute value of Stokes *V* (in units of the continuum intensity) over 100 nm bins of the solar-like model. Solid: 100 G. Dashed: 1000 G. Dotted: 5000 G. The scale of the dashed (dotted) curve has been reduced by a factor of 10 (30) in order for all three curves to be plotted together.

**Table 2.** Compilation of spectral line pairs with identical line opacities.

| Ion | Wavelength (nm) | Excitation potential (eV) | $\log(gf)$ | $\bar{g}_{\text{eff}}$ |
|---|---|---|---|---|
| Fe I | 400.560 | 4.186 | −2.131 | 2.0000 |
| Fe I | 453.894 | 4.186 | −2.131 | 0.8333 |
| Fe I | 402.473 | 3.241 | −0.710 | 0.6250 |
| Fe I | 408.530 | 3.241 | −0.710 | 1.7083 |
| Ti I | 406.509 | 1.053 | −0.760 | 1.5000 |
| Ti I | 469.876 | 1.053 | −0.760 | 1.0000 |
| V I | 410.516 | 0.267 | −0.130 | 1.5000 |
| V I | 440.851 | 0.267 | −0.130 | 1.4667 |
| Fe I | 412.180 | 2.832 | −1.300 | 0.6667 |
| Fe I | 899.956 | 2.832 | −1.300 | 1.5000 |
| Na I | 421.606 | 2.104 | −2.350 | 1.1000 |
| Na I | 454.518 | 2.104 | −2.350 | 1.1667 |
| Fe I | 428.582 | 3.640 | −1.780 | 1.1667 |
| Fe I | 496.870 | 3.640 | −1.780 | 0.8333 |
| Ca I | 435.508 | 2.709 | −0.430 | 1.0000 |
| Ca I | 452.693 | 2.709 | −0.430 | 1.0000 |
| Fe I | 443.834 | 3.686 | −1.630 | 2.5000 |
| Fe I | 466.806 | 3.686 | −1.630 | 1.7500 |
| Mn I | 445.301 | 2.941 | −0.490 | 1.5000 |
| Mn I | 473.909 | 2.941 | −0.490 | 0.8000 |
| Fe I | 456.531 | 3.274 | −2.510 | 2.0000 |
| Fe I | 479.125 | 3.274 | −2.510 | 0.5000 |
| Fe I | 457.982 | 3.071 | −2.830 | 1.7500 |
| Fe I | 718.915 | 3.071 | −2.830 | 1.0000 |
| Fe I | 461.929 | 3.603 | −1.120 | 1.8333 |
| Fe I | 463.801 | 3.603 | −1.120 | 1.7917 |
| Fe I | 463.585 | 2.845 | −2.420 | 2.2500 |
| Fe I | 635.503 | 2.845 | −2.420 | 1.0000 |
| Ti I | 469.133 | 1.067 | −0.840 | 1.1667 |
| Ti I | 586.645 | 1.067 | −0.840 | 1.1667 |
| Fe I | 480.065 | 4.143 | −1.260 | 1.0000 |
| Fe I | 518.792 | 4.143 | −1.260 | 1.0000 |
| Si I | 540.466 | 5.614 | −0.530 | 2.0000 |
| Si I | 548.898 | 5.614 | −0.530 | 2.0000 |
| Si I | 540.466 | 5.614 | −0.530 | 2.0000 |
| Si I | 623.732 | 5.614 | −0.530 | 2.0000 |
| Si I | 540.985 | 5.616 | −0.690 | 2.0000 |
| Si I | 624.447 | 5.616 | −0.690 | 2.0000 |
| Si I | 548.898 | 5.614 | −0.530 | 2.0000 |
| Si I | 623.732 | 5.614 | −0.530 | 2.0000 |
| Fe I | 560.294 | 3.430 | −0.851 | 0.7500 |
| Fe I | 565.853 | 3.430 | −0.851 | 2.2500 |
| Si I | 565.492 | 5.614 | −0.930 | 2.0000 |
| Si I | 612.502 | 5.614 | −0.930 | 2.0000 |

region from 400 to 500 nm exhibits nearly as much signal as the rest of the spectrum combined (from 500 to 1600 nm). The reason for this is two-fold. First, the blue region is heavily crowded with a large number of closely packed spectral lines. This is evident from Table 1, where we can see that the number of lines per wavelength interval decreases monotonically towards longer wavelengths. Second, blue lines are typically much stronger than red or infrared lines. The degree of polarization produced by a Zeeman-split line depends not only on the magnetic field and the component splitting, but also on the line strength.

We can see in Fig. 3 the balance among all the different effects for this model. The amount of Stokes *V* signal is largest at 400 nm and decreases monotonically across the visible spectrum. A minimum is reached between 1200 and 1300 nm, after which the three curves start to increase again all the way up to 1600 nm. For the stronger fields, the signal drop with wavelength is considerably more pronounced and the increase after 1300 nm is much weaker. This is because the amount of polarization produced by a line increases with the field strength only in the so-called *weak-field regime* (see, e.g., Landi Degl'Innocenti 1992). This is the regime in which the Zeeman splitting is smaller than the Doppler width of the line. If all other parameters are constant, the ratio of Zeeman splitting to Doppler width increases linearly with wavelength. As we increase the field strength, red and infrared lines are more likely to depart from the weak-field regime before blue lines do. In the saturation regime, the polarization amplitude does not increase with the magnetic field any more. In summary, observing longer wavelengths is only advantageous (in terms of polarization amplitude) for relatively weak fields (~100 G).

If the magnetic field is not homogeneous and covers only a fraction of the stellar surface, then the Stokes *V* spectrum will have its overall amplitude decreased according to the *filling factor* (fractional surface area occupied by the magnetic field). Generally, it is not straightforward to separate the field strength from its filling factor. Figure 3 gives us a clue on how this might be accomplished, since the shapes of the curves for different intrinsic field strengths are clearly different. If one were to take the ratio of polarization signal in the 800 nm to the 400 nm band, this ratio would be larger for the weaker fields and decrease as

the field becomes stronger. This is a similar concept to the line-ratio technique used by Stenflo (1973) to propose that the solar magnetic network is actually composed of strong kG fields occupying small filling factors.

There are many other lines that could potentially be used to disentangle intrinsic field strength from filling factor. Table 2 lists a number of spectral lines that have the same line opacity (same lower level excitation potential and $\log(gf)$). The Fe I lines at 412.180 and 899.956 nm are particularly promising (see Socas-Navarro et al. 2006), although the disparity in wavelength may introduce complications (most notably, the background opacities are sensibly different). There is a number of Fe I, Ca I, Ti I and Si I that also have the same Landé factor, and are therefore virtually identical except for their wavelength. These lines may be useful, for example to determine accurate atmospheric temperatures through the calculation of their equivalent width ratio.

**Table 3.** Wavelengths (in nm) exhibiting strongest polarization in the solar-like model. The numbers in parenthesis give the degree of polarization (relative to the local continuum).

| 100 G | 1000 G | 5000 G |
|---|---|---|
| 1159.34 (7.18%) | 525.02 (35.38%) | 448.97 (44.36%) |
| 846.83 (6.56%) | 423.27 (34.63%) | 420.66 (44.13%) |
| 1449.77 (6.27%) | 425.83 (34.21%) | 411.17 (43.63%) |
| 525.02 (5.94%) | 524.75 (33.64%) | 431.28 (43.37%) |
| 1564.84 (5.78%) | 408.08 (33.62%) | 400.16 (43.24%) |
| 1386.41 (5.74%) | 513.14 (33.36%) | 417.49 (43.11%) |
| 1168.98 (5.71%) | 461.33 (33.33%) | 408.29 (43.02%) |
| 1142.22 (5.45%) | 454.59 (31.96%) | 412.12 (42.67%) |
| 1456.57 (5.45%) | 550.67 (31.95%) | 429.14 (42.65%) |
| 513.14 (5.38%) | 522.55 (31.89%) | 457.10 (42.55%) |
| 524.75 (5.37%) | 448.56 (31.66%) | 437.44 (42.55%) |
| 525.01 (5.26%) | 429.14 (31.10%) | 438.92 (42.53%) |
| 1399.74 (5.25%) | 465.44 (30.81%) | 405.55 (42.43%) |

Table 3 lists the wavelengths with strongest polarization signal in the solar-like model. We can see that for weak fields the strongest signals are in the infrared. As the field strength increases, most of the infrared lines saturate and the strongest signals are observed in shorter wavelengths. Note that it is not straightforward in general to associate specific spectral lines to those wavelengths because some times (especially in the blue), the polarization signal arises from a blend of several lines. For example, the strongest signal in the solar spectrum produced by weak fields (~100 G) comes from a Fe I line with central wavelength at 1159.358 nm with an effective Landé factor of 2.5. For very strong fields, on the other hand, the strongest signal comes from a very crowded region around 448.97 nm. Figure 4 shows the Stokes $V$ profile in this region. The most conspicuous feature is produced mostly by an Fe I line at 448.9739 nm (vertical dotted line), but there are other lines with very close wavelengths that contribute to it.

The variation with spectral type is shown in Fig. 5 for $\log(g) = 4.5$. The later spectral types (left of the figure) have a very prominent blue side of the spectrum, with a steep decrease towards the red. Earlier types exhibit a rather flat spectral dependence, with a minimum around 700 nm. Notice also that there is an overall decrease of the polarization signal for hotter stars. This is due to a combination of three different physical effects. First, the thermal broadening of spectral lines increases with $T_{\mathrm{eff}}$, smearing out the polarization signal. Second, the increase in excitation and ionization state of the atoms in the plasma reduces the number and strength of spectral lines (especially, the abundant low-excitation Fe1 lines). This effect is particularly important in the blue. Finally, if we compute the source function ($S$) and its gradient ($\mathrm{d}S/\mathrm{d}\tau$) and plot the ratio ($\mathrm{d}S/\mathrm{d}\tau$)/$S$ in the photosphere as a function of $T_{\mathrm{eff}}$, we find that this ratio has a maximum around 5000 K and then decreases monotonically for hotter stars.

## 4. Conclusions

Stellar polarimetry is becoming increasingly important in Astrophysics and it is now possible to obtain polarized spectra over a broad range of wavelengths (examples are the Narval and Musicos instruments at Pic du Midi, Aurière 2003; or ESPaDOnS at the Canada-France-Hawaii Telescope, Petit et al. 2003), or over a narrower range with very high spatial
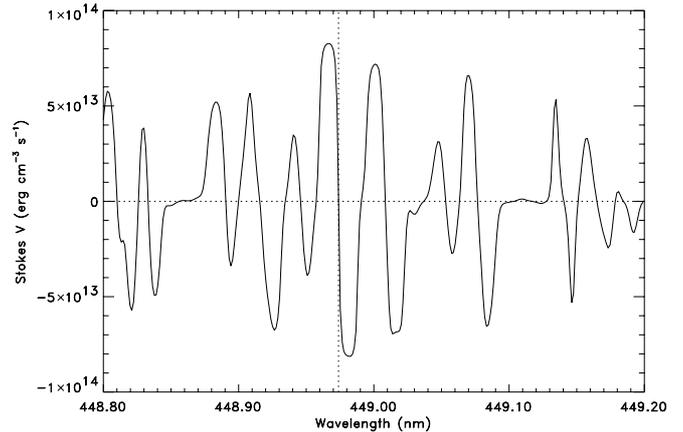


**Fig. 4.** Stokes $V$ signal in the region around 449 nm. This is where the strongest polarization is found for the 5000 G field. The vertical dotted line marks the central wavelength of a strong Fe I transition at 448.9739 nm. The half-amplitude of this profile is approximately 44% of the continuum intensity.

resolution and large aperture (FORS at the VLT; e.g., Hubrig et al. 2004a,b).

We have used a Stokes synthesis code and a large array of LTE models to produce an atlas of the polarization signal expected from a wide variety of magnetic stars. We hope that this tool will be useful for the planning of future polarimetric observing runs and perhaps for the interpretation of the data, as well.

For example, it may be possible to (coarsely) generalize the popular least-squares deconvolution technique (Donati et al. 1997) to intermediate and strong magnetic regimes. In order to do this, one would take the atlas for the specific star under consideration and add all the spectral lines together, as is usually done when applying least-squares deconvolution, for different magnetic field strengths. By comparing the observed profile to those obtained from the atlas, we may be able to estimate the stellar magnetic field.

In principle, it is conceivable to use the synthesis module developed here for the application of least-squares inversions (e.g., Socas-Navarro 2001; del Toro Iniesta 2003) to stellar spectropolarimetric observations. It would be a siginifcant computational undertaking, however, since this kind of inversions typically requires of the order of ~100 syntheses (or, if one wishes to use numerical response functions, this figure would have to be multiplied by the number of free parameters). An interesting alternative may be the use of inversions based on Principal Component Analysis combined with a look-up algorithm (Rees et al. 2000; Socas-Navarro et al. 2001; Semel et al. 2006). To this aim, it would be desirable to develop a more refined grid with a better sampling of the magnetic field and, possibly, a variety of geometries.

A final caveat in using our atlas is that it has been derived from a very simple magnetic toplogy. Active stars are likely to exhibit more complex magnetic structuring. The integration of different field orientations over the stellar disk would result in an overall decrease of the circular polarization signal with respect to the synthetic profiles presented here. However, the relative scaling between different lines and spectral regions should be approximately correct.
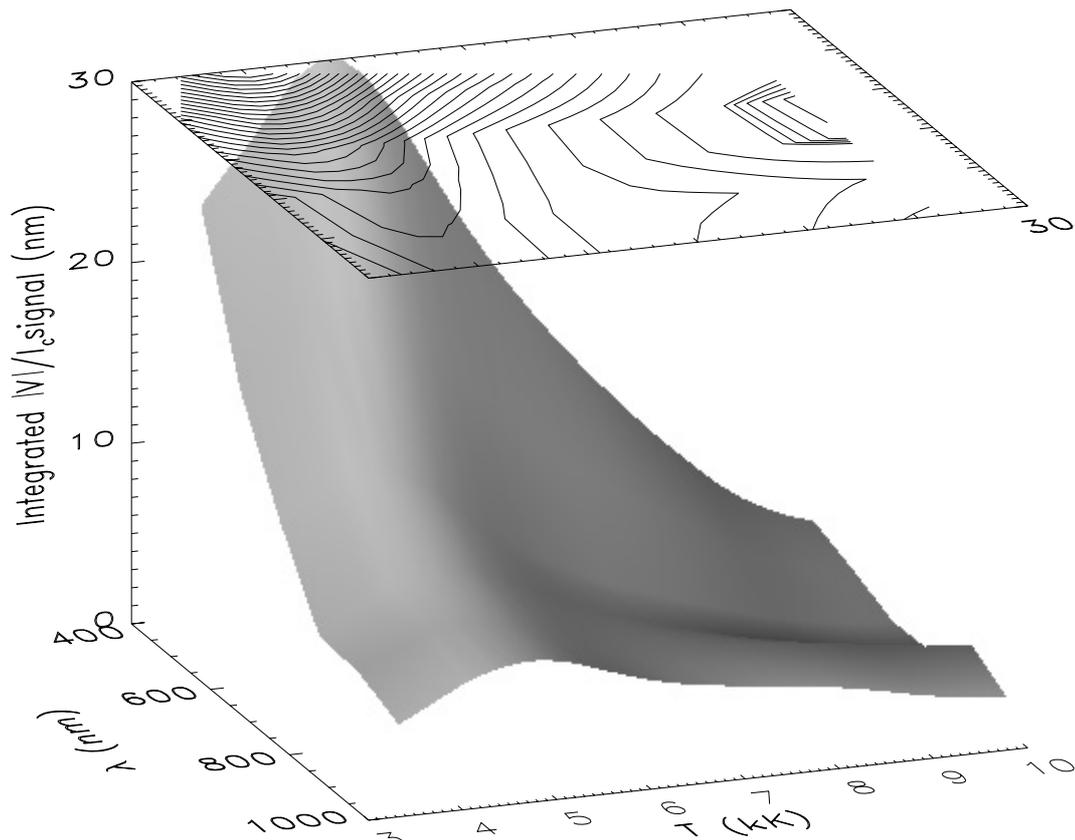
**Fig. 5.** Integrated absolute value of Stokes $V$ (in units of the continuum intensity) over 100 nm bins for varying spectral types and a 1 kG field.

# References

Allende Prieto, C., García López, R., Lambert, D. L., & Ruiz Cobo, B. 2000, ApJ, 528, 885

Anders, E., & Grevesse, N. 1989, Geochim. Cosmochim. Acta, 53, 197

Aurière, M. 2003, in EAS Publications Series, ed. J. Arnaud, & N. Meunier, 105

Bellot Rubio, L. R., Ruiz Cobo, B., & Collados, M. 1998, ApJ, 506, 805

Casini, R., & Landi Degl'Innocenti, E. 1994, A&A, 291, 668

Castelli, F., & Kurucz, R. L. 2003, in IAU Symp. 20, ed. N. Piskunov, W. W. Weiss, & D. F. Gray

Castelli, F., Gratton, R. G., & Kurucz, R. L. 1997a, A&A, 324, 432

Castelli, F., Gratton, R. G., & Kurucz, R. L. 1997b, A&A, 318, 841

del Toro Iniesta, J. C. 2003, Astron. Nachr., 324, 383

Donati, J.-F., Catala, C., Wade, G. A., et al. 1999, A&AS, 134, 149

Donati, J.-F., Semel, M., Carter, B. D., Rees, D. E., & Collier Cameron, A. 1997, MNRAS, 291, 658

Donati, J.-F., Paletou, F., Bouvier, J., & Ferreira, J. 2005, Nature, 438, 466

Gray, D. F. 1976, The observation and analysis of stellar photospheres, Research supported by the National Research Council of Canada (New York: Wiley-Interscience)

Hales, A. S., Gledhill, T. M., Barlow, M. J., & Lowe, K. T. E. 2006, MNRAS, 365, 1348

Hubrig, S., Kurtz, D. W., Bagnulo, S., et al. 2004a, A&A, 415, 661

Hubrig, S., Schöller, M., & Yudin, R. V. 2004b, A&A, 428, L1

Humlicek, J. 1982, JQSRT, 27, 437

Keller, C. U. 2006, in Ground-based and Airborne Instrumentation for Astronomy, ed. I. S. McLean, & M. Iye, Proc. SPIE, 6269

Kurucz, R., & Bell, B. 1995, Atomic Line Data, ed. R. L. Kurucz, & B. Bell, Kurucz CD-ROM No. 23, Cambridge (Mass.: Smithsonian Astrophysical Observatory)

Landi Degl'Innocenti, E. 1992, in Solar Observations: Techniques and Interpretation, First Canary Islands Winter School of Astrophysics, ed. F. Sánchez, M. Collados, & M. Vázquez (Cambridge Univ. Press), 71

Landi Degl'Innocenti, E., & Landolfi, M. 2004, Polarization in Spectral Lines (Kluwer Academic Publishers)

Landi degl'Innocenti, E., Landi Degl'Innocenti, M., & Landolfi, M. 1988, A&A, 204, 133

Manset, N., & Donati, J.-F. 2003, in Polarimetry in Astronomy, ed. S. Fineschi, Proc. SPIE, 4843, 425

Perrin, M. D., Duchêne, G., Kalas, P., & Graham, J. R. 2006, ApJ, 645, 1272

Petit, P., Donati, J.-F., & The Espadons Project Team 2003, in EAS Publ. Ser., ed. J. Arnaud, & N. Meunier, 97

Rees, D., López Ariste, A., Thatcher, J., & Semel, M. 2000, A&A, 355, 759

Sánchez Almeida, J., & Trujillo Bueno, J. 1999, ApJ, 526, 1013

Semel, M., Rees, D. E., Ramírez Vélez, J. C., Stift, M. J., & Leone, F. 2006, in ASP Conf. Ser., 358, Solar Polarization 4, ed. R. Casini, & B. W. Lites, in press

Shakhovskoj, D., Grinin, V., Rostopchina, A., et al. 2006, A&A, 448, 1075

Shchukina, N., & Trujillo Bueno, J. 2001, ApJ, 550, 970

Socas-Navarro, H. 2001, in Advanced Solar Polarimetry – Theory, Observation, and Instrumentation, ASP Conf. Ser., 236, 487

Socas-Navarro, H., Borrero, J., Asensio Ramos, A., et al. 2006, ApJ, in preparation

Socas-Navarro, H., López Ariste, A., & Lites, B. W. 2001, ApJ, 553, 949

Stenflo, J. O. 1973, Sol. Phys., 32, 41

Trujillo Bueno, J., Moreno-Insertis, F., & Sánchez, F. 2002, Astrophysical Spectropolarimetry, XII Canary Islands Winter School of Astrophysics (Cambridge University Press)

Wade, G. A., Drouin, D., Bagnulo, S., et al. 2005, A&A, 442, L31